International Journal of Solids and Structures 48 (2011) 687–697

Contents lists available at ScienceDirect

International Journal of Solids and Structures

journal homepage: www.elsevier.com/locate/ijsolstr

Impact behavior of honeycombs under combined shear-compression. Part I: Experiments

B. Hou [a,b], A. Ono [c], S. Abdennadher [c], S. Pattofatto [b], Y.L. Li [a], H. Zhao [b,*]

[a] School of Aeronautics, Northwestern Polytechnical University, 710072 Xi'an, China
[b] Laboratoire de Mecanique et Technologie, ENS Cachan/CNRS UMR8535/UPMC Paris universitas/PRES UniverSud, 61 Avenue du président Wilson, 94235 Cachan Cedex, France
[c] MEDYSYS 6, Bd Dubreuil, 91400 Orsay, France

ARTICLE INFO

Article history:
Received 25 March 2010
Received in revised form 3 October 2010
Available online 5 November 2010

Keywords:
Honeycombs
Combined shear-compression
Hopkinson bars
Dynamic strength enhancement

ABSTRACT

This paper presents a combined shear-compression impact test for soft cellular materials designed in order to investigate their behavior under impact multiaxial loadings. A large-diameter Nylon Split Hopkinson Pressure Bar system (SHPB) with beveled ends of different angles is used to apply the desired shear-compression combinations. The data processing methods are studied and validated by virtual testing data generated with FEM simulations. A series of experiments on an aluminum honeycomb were performed at the impact velocity of about 15 m/s with the loading angles ranging from 0° (corresponding to the pure compression) to 60°. It shows a strong effect of the additional shear loading because both the initial peak and the crush strength decrease with increasing loading angles. The quasi-static shear-compression experiments were also performed using the same beveled ends on a universal INSTRON machine and a notable strength enhancement under impact loading is observed. Images captured during quasi-static and impact tests permit for the determination of the two co-existing deforming patterns under combined shear-compression and reveal the influence of the loading rate on the occurrence of these two patterns.

1. Introduction

Honeycombs as well as the other cellular materials are commonly used for energy absorption designs in aerospace and modern vehicle applications. Their mechanical behaviors were extensively studied under various quasi-static loadings (Wierzbicki, 1983; Zhang and Ashby, 1992). Under impact loading conditions, which are the real working condition for energy absorbing systems made of cellular materials, only a few investigations limited to uniaxial compression are reported in the open literatures (Wu and Jiang, 1997; Zhao and Gary, 1998; Goldsmith and Louie, 1995; Zhao et al., 2005). Experimental investigations of cellular materials under dynamic multiaxial loading are not available as yet. The main reason for such situations lies in the difficulties to perform dynamic multiaxial experiments because of the requirements for both a feasible multiaxial design in a tiny limited space and an accurate data measurement under these conditions.

In the past decade, various multiaxial quasi-static loading methods suitable for cellular material were developed (Papka and Kyriakides, 1999; Deshpand and Fleck, 2001; Chung and Waas, 2002; Chen and Fleck, 2002; Mohr and Doyoyo, 2003; Mohr and Doyoyo, 2004; Kintscher et al., 2007; Hong et al., 2006; Hong et al., 2008; Karagiozova and Yu, 2008). For example, Papka and Kyriakides (1999), and Chung and Waas (2002) employed a quasi-static biaxial loading machine to investigate the in-plane biaxial compression properties of honeycombs. In their facilities, the specimen was placed between two pairs of loading platens which could move independently in two orthogonal directions. Mohr and Doyoyo (2003) modified the standard Arcan apparatus using a clamped configuration to restrict the rotations of the grips and tested the combined out-of-plane shear-compression behavior of honeycombs. They estimated possible errors of ignoring the additional horizontal force produced by the clamped configuration (Mohr and Doyoyo, 2002) and integrated another load cell to measure it. Mohr and Doyoyo (2004) also had another universal biaxial testing device which employed three load cells to measure the forces in two different directions. Based on a Zwick static test facility, Kintscher et al. (2007) developed a test device with the combination of a roll and a steel towing rope to apply combined out-of-plane shear-compression to a folded sandwich double-core specimen. Hong et al. established two systems (so-called the independently controlled test fixture (Hong et al., 2006) and the inclined test fixture (Hong et al., 2008)) to perform the quasi-static biaxial experiment on honeycombs. These aforementioned quasi-static biaxial loading methods succeed in measuring the in-plane

* Corresponding author. Tel.: +33 1 47 40 20 39; fax: +33 1 47 40 22 40.
E-mail address: zhao@lmt.ens-cachan.fr (H. Zhao).

0020-7683/$ - see front matter © 2010 Elsevier Ltd. All rights reserved.
doi:10.1016/j.ijsolstr.2010.11.005

biaxial or combined out-of-plane shear-compression behavior of honeycombs by using more than one load cell.

As to dynamic multiaxial experiments, on the one hand, some studies using the drop-weight or high-speed machine have been reported. For example, Chung and Waas (2002) introduced biaxial loading by restricting the transversal displacement of the specimen while dropping the weight. The only found combined dynamic out-of-plane shear-compression test on honeycomb was achieved by Hong et al. (2008). They designed an impact test fixture based on their quasi-static method to introduce combined dynamic shear-compressive loading. The projectile was designed to strike a complex load transfer unit in order to generate a nearly constant loading velocity. A multiaxial load cell was used to measure the normal and shear loads applied to the specimen. These methods in a drop-weight frame or high-speed testing machine system might suffer from a rather poor measurement accuracy at higher loading rates.

On the other hand, the Split Hopkinson pressure bar technique provides a more precise method for testing the material behavior under higher loading rates. Nowadays, it is not only used for standard uniaxial test, but also can be modified and adapted to develop multiaxial dynamic testing in many special cases (Gary and Bailly, 1998; Rittel et al., 2002; Chen and Ravichandran, 1997; Nie et al., 2007).

In this study, we try to combine the advantages of aforementioned techniques and to propose a new testing method to perform the combined dynamic shear-compression tests using a large-diameter (Φ = 60 mm) Nylon SHPB bars. It is based on two short beveled bars (with various inclined angles from 30° to 60°) made of the same material and with the same diameter as the Hopkinson bars. In Part I of this study, the design as well as the FEM analyses of the whole loading system will be presented. Such FEM analyses allow to ensure the accuracy of the global force and velocity measurement given by those beveled SHPB bars. A series of experiments at loading angles ranging from 0° (corresponding to pure compression) to 60° are performed at impact velocities of about 15 m/s and the overall pressure/crush curves under various shear-compression combinations are obtained. The numerical simulations and analyses of the combined shear-compression behavior of honeycombs under impact loading will be discussed in Part II of this study.

2. Combined shear-compression setup using 60 mm Nylon SHPB

2.1. Nylon SHPB and soft cellular material testing

The SHPB is nowadays a popular tool for material behavior characterization under impact loading (Hopkinson, 1914; Kolsky, 1949). Initially developed for metallic material testing, it has now been adapted for many different materials (Zhao, 1998; Zhao, 1997). In order to characterize soft cellular materials, soft large-diameter viscoelastic bars are used to provide a larger cross section and a better impedance match. Indeed, the large-diameter improves the sample/cell size ratio and reduces the data scatter. Meanwhile, a better impedance match enhances the small signal/noise ratio due to the low strength of soft cellular materials. The use of such large-diameter viscoelastic Nylon bars requires some precautions in the wave-shift procedure because of the wave propagation in the viscoelastic bars and the non-negligible geometrical wave dispersion due to larger bar diameter (Zhao et al., 1997). Successful compressive testing on various soft cellular materials using this technique can be found in the open literature (Zhao et al., 1997). In the present study, a 60 mm diameter SHPB setup (2×3 m long Nylon bar) is used as basic loading and measuring techniques.

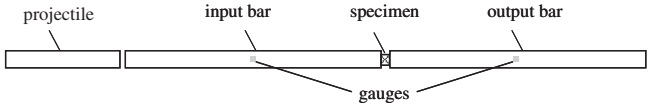

Fig. 1. SHPB set-up.

A typical SHPB set-up is shown in Fig. 1. A projectile launched by a gas gun strikes the free end of the input bar and develops a compressive longitudinal incident wave $\varepsilon_i(t)$. Once this wave reaches the bar/specimen interface, part of it $\varepsilon_r(t)$, is reflected, whereas the other part goes through the specimen and develops the transmitted wave $\varepsilon_t(t)$ in the output bar. Two gauges are cemented at the midpoints of input and output bars to record those three basic waves which can be used to investigate the constitutive behavior of the specimen.

2.2. Combined shear-compression set-up

In order to introduce combined shear-compressive loading, two short cylindrical bars with one bevel end are put at the interfaces of the specimen and the input and output bars. Fig. 2(a) and (b) shows the scheme and a photograph of our combined dynamic shear-compression device. The two inserted short beveled bars are made of the same material and have the same diameter as the Hopkinson bars. This insures that the incident wave propagates from the input bar to the input beveled bar without significant reflection, and the transmitted wave can also travel from the output beveled bar to the output bar completely. The honeycomb specimen is placed between the two parallel bevels instead of contacting with the input and output bars directly and perpendicularly. A column sleeve made of Teflon and two aluminum supports are used to fix the whole device.

It is worth emphasizing that the friction coefficient between the specimen and the beveled bars should be large enough to make

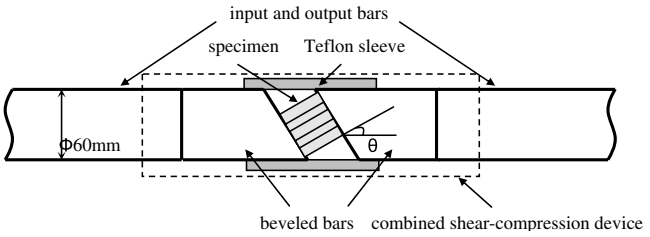

(a)

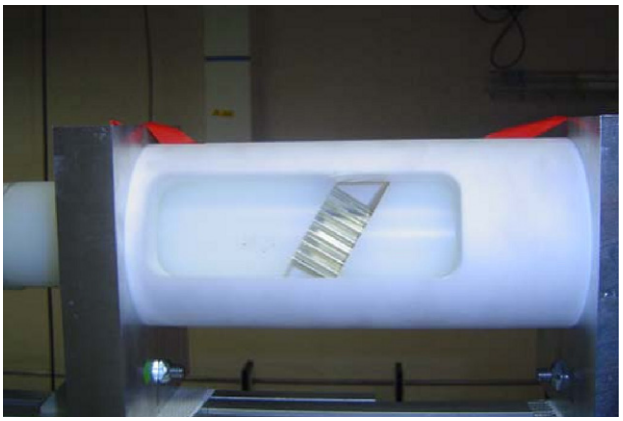

(b)

Fig. 2. Scheme and photograph of the dynamic biaxial loading device.

sure that no slippage occurs during the loading period. In this way, when the specimen is loaded by the horizontal movement of input and output bevels, a combined shear-compressive loading state is achieved. For the sake of illustration convenience, loading angle θ is defined as the angle between the axes of honeycomb cells and the loading direction (as shown in Fig. 2(a)). Clearly, the larger the loading angle is, the more dominant the shear component is. When $\theta = 0°$, a pure compressive experiment is obtained.

2.3. Elementary data processing

Instead of using classical SHPB formulas which lead directly to average stress/strain curve under the assumption of homogeneous stress/strain field within the specimen, here we use the SHPB only as loading and measuring system. According to the theory of elastic (viscoelastic) wave propagation, the stress and the particle velocity of a single wave can be accurately determined from the associated strain measured by strain gauges. Furthermore, these quantities are not only known at the points of strain gauges, but at any point on the bar. Thus, forces and velocities at the interfaces of the bar/specimen can be obtained by the local strain signals shifted from the measuring points. The associated forces and particle velocities are then calculated as follows:

$$\begin{aligned} F_{input}(t) &= S_b E(\varepsilon_i(t) + \varepsilon_r(t)) \quad & V_{input}(t) &= C_0(\varepsilon_i(t) - \varepsilon_r(t)) \\ F_{output}(t) &= S_b E\varepsilon_t(t) & V_{output}(t) &= C_0\varepsilon_t(t) \end{aligned} \tag{1}$$

where F_{input}, F_{output}, V_{input} and V_{output} are forces and particle velocities on specimen faces. S_b, E and C_0 are respectively the cross section area, Young's modulus of the bars and the longitudinal wave speed. $\varepsilon_i(t)$, $\varepsilon_r(t)$, $\varepsilon_t(t)$ are the wave signals at the bar/specimen interfaces.

For the viscoelastic bars, the commonly used method is to correct the wave shape change on propagation but neglect locally the shape difference among stress, strain and particle velocity, so that the Eq. (1) is still used here (Zhao et al., 1997).

Fig. 3(a) shows the input and output forces as a function of time at $\theta = 30°$. An obvious difference between these two forces is observed in the initial region, where equilibrium is not reached yet, but this difference is largely reduced at the subsequent plateau stage ($t > 0.4$ ms). The input and output velocities depicted in Fig. 3(b) shows that the crushing rate is rather constant during the test.

As a stress/strain homogeneous field assumption is not really valid in our case of soft cellular materials with localized deformation mechanism, we use only the mean pressure $p(t)$ as a function of the overall crush $\Delta(t)$ to give an overall idea of the behavior of this kind of material (Zhao and Gary, 1998). They are defined as:

$$\begin{aligned} p(t) &= F_{input}(t)/S_s \\ \Delta(t) &= \int_0^t (V_{output}(\tau) - V_{input}(\tau))d\tau \end{aligned} \tag{2}$$

where S_s is the apparent area of the specimen face contacting to the beveled bars.

The use of the input force here is motivated by the fact that the output force may contain more experimental errors such as the friction between Teflon sleeve and beveled bars, an imperfect contact between bar/specimen and a bad alignment etc. Thus, the input force is believed to be more accurate. The simulation work in Part II shows also that the input force can be easily reproduced while the output force is difficult to simulate in an idealized testing condition.

The pressure/crush curve of honeycomb specimen for this test is obtained and shown in Fig. 3(c). Such an average pressure/crush curve gives an overall prediction of the dynamic multiaxial behavior of tested specimen under combined shear-compression.

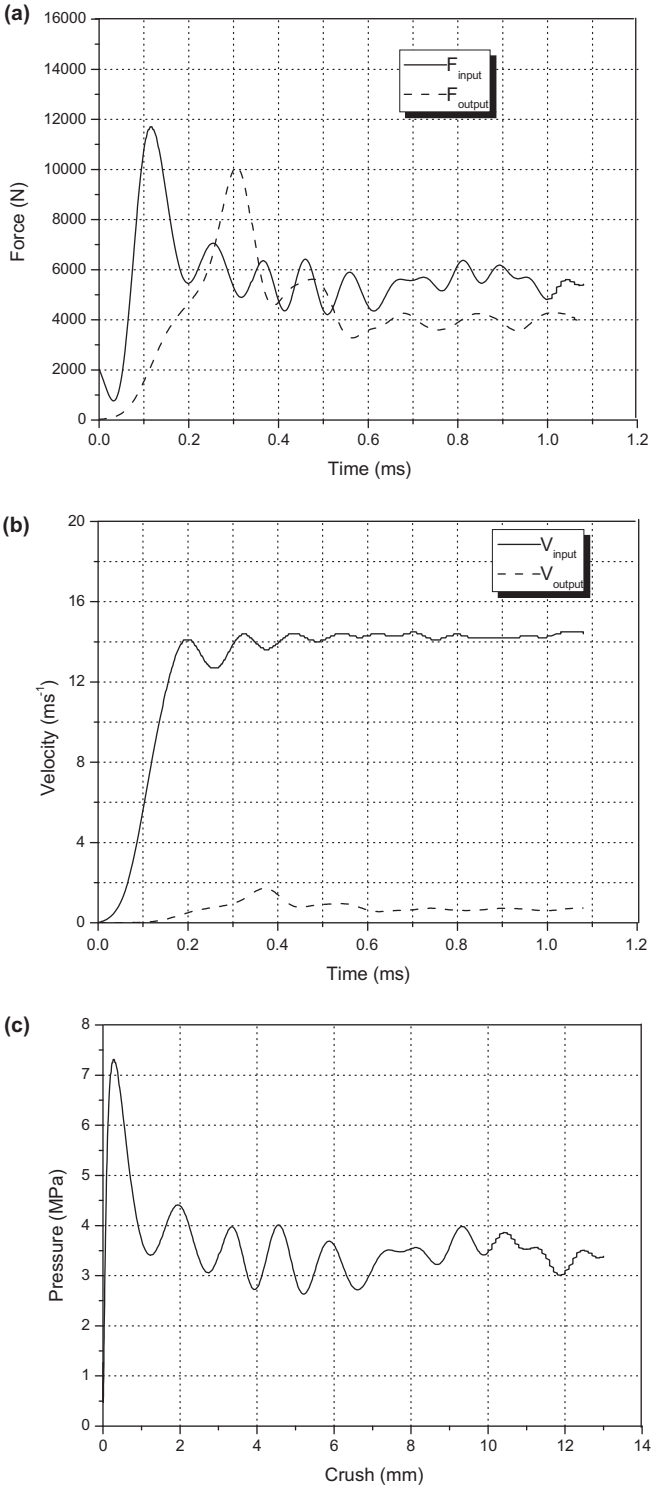

Fig. 3. Forces (a), velocities (b) and pressure/crush curve (c) in a combined test at $\theta = 30°$.

3. Validation of the combined shear-compression measuring method

The validity of the overall pressure/crush curve obtained in Section 2 is based on the assumption that the velocities at any material point on the inclined section at the beveled ends are rather identical and that the elastic strain during loading is small enough to be

neglected. It also implies that the friction force between the beveled bar of the input side and the Teflon sleeve is very small so that the axial force supported by the specimen is fully transmitted to the input bar. In order to verify these assumptions and to evaluate the potential errors, a numerical analysis of the whole loading system is performed. Such a virtual numerical test allows for the comparison between the forces and the velocities derived from the strain history at the measuring point in the pressure bars and these located at the interfaces between beveled bar ends and specimen faces.

A virtual experiment using the finite element method is performed via ABAQUS/Explicit in order to clarify these uncertainties. We established an entire model using the actual size of experimental apparatus, composed of the projectile, input and output bars, inserted beveled bars, Teflon sleeve and specimen, to simulate the whole loading process. The angle of the beveled bars is 30° for this computation.

The geometrical model was discretized by 8-node linear brick elements with reduced integration and hourglass control (C3D8R). An element size of 0.5 mm was chosen for the bars and Teflon sleeve, while for the bevels and specimen, smaller elements with sizes of 0.3 mm and 0.15 mm were used respectively. A convergence study on element size shows that the used elements are small enough for obtaining reliable results within reasonable calculation expense. With the used element sizes, the model has 164,316 elements in total. A part of the meshed FEM model around the biaxial loading device area is shown in Fig. 4.

A crushable foam model available in this code (see section 18.3.5, Abaqus Analysis User's Manual) is chosen to describe the constitutive behavior of the specimen. The parameters are identified with the experimental data of the studied honeycomb under quasi-static pure compression (the pressure/crush curve is shown in Fig. 5). In fact, as the specimen takes only a small part in the whole model, its elastic part (Young's Modulus, Poisson Ratio) is not very important in the calculation. Under plastic regime, the Poisson's ratio is set to zero and lock strain is determined rather roughly. The only dominant parameter σ_s is defined as the average level shown in Fig. 5. For the other parts of the model, linear material with elastic constants of Nylon and Teflon is used for bars and sleeve respectively. All the material parameters are listed in Table 1.

Surface-to-surface contact with penalty contact method is employed for all the contacts. At the interfaces between the specimen and the beveled bars, a no sliding condition is applied. The interfaces between Nylon bars and bevels are given frictionless contact property. The friction force between the Teflon sleeve and the Nylon bevels is estimated with the penalty friction formulation and the friction coefficient is set to be 0.05.

The projectile has an initial velocity of 30 m/s in axial (X_3) direction which is the real impact velocity measured in our experiment.

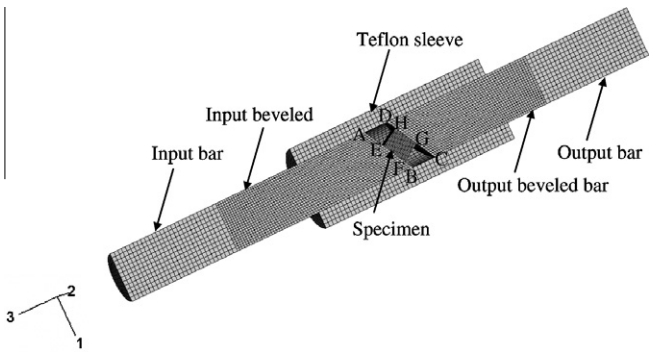

Fig. 4. Finite element model (view cut by X_1X_3 plane).

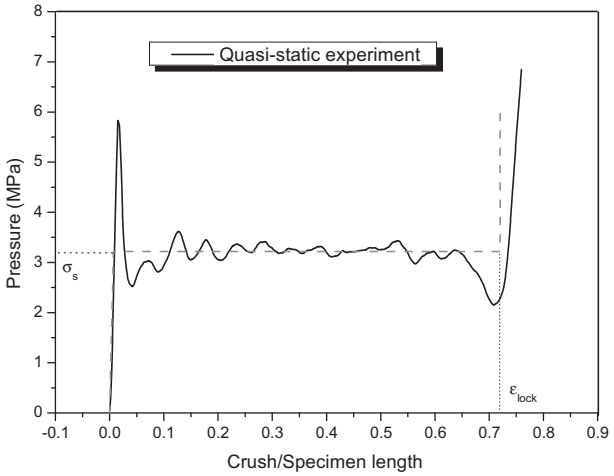

Fig. 5. Pressure/crush curve under quasi-static uniaxial compression.

The external surface of the Teflon sleeve is restricted on three translational displacements. For the Hopkinson bars, lateral displacements (in the X_1 and X_2 directions) are restricted on their external surface at four sections corresponding to the positions of the supports.

Two nodes located on the external surface of the input and output bars corresponding to the positions of strain gauges are picked. The strain component (LE_{33}) in the axial (X_3) direction at these two nodes is shown in Fig. 6.

Fig. 7 shows the comparison between the calculated strain signals and the experimental ones. The incident and reflected waves from experiments and simulation are rather in good agreement. The large oscillations in the simulated incident and reflected waves are, for a large amount, due to elastic bars assumption in simulation. In the real test, the oscillation is smaller because of the viscoelastic feather of the bars which tend to generate less oscillating incident wave. However, such oscillations do not affect the main feature (movement and stress) of beveled ends. For the transmitted wave, there is some difference, especially for the peak value, which may imply some imperfect contact or alignment in the real test.

In order to validate the accuracy of the force measurement and to estimate the influence of friction between the beveled bars and the Teflon sleeve, the following quantities are extracted from simulation data. The force derived from the bar F_{bar} is obtained from the strain on the input bar using the data process method of SHPB (Eq. (1)). The force at the bar/specimen interface $F_{specimen}$ is the X_3 component of total force due to the contact pressure and the frictional stress between specimen and input bevel which can be picked up directly in simulation. The friction force $F_{friction}$ is the X_3 component of total force due to friction between input bevel and Teflon sleeve.

Fig. 8 shows the comparison between these three quantities, indicating that $F_{friction}$ is a small value comparing with F_{bar} and $F_{specimen}$ and can be neglected without leading to significant error on them.

In order to verify the assumption of identical axial displacements of beveled ends, we depict the axial displacements for the positions located at longer major axe of ellipse of bevels at the instant when the specimen strain is maximal. In Fig. 9, the positions A, B, C and D correspond to the four free end nodes and E, F, G, H are the four edge contact points between specimen and bevels (Fig. 4). A displacement difference of 0.17 mm between the contact region of specimen and free end nodes of bevels is observed, which approximately results in an error of 1.31%.

Table 1
Material parameters used in the simulations.

	Density ρ(kg/m^3)	Young's Modulus E (MPa)	Poission's Ratio v	Plastic Possion's Ratio v_p	Yield Stress σ_s (MPa)	Lock Strain ε_{lock}
Honeycomb	82.6	450	0.35	0	3.22	0.72
Nylon	1120	3370	0.3	–		
Teflon	2200	1500 (Rae and Dattelbaum, 2004)	0.46 (Rae and Dattelbaum, 2004)	–		

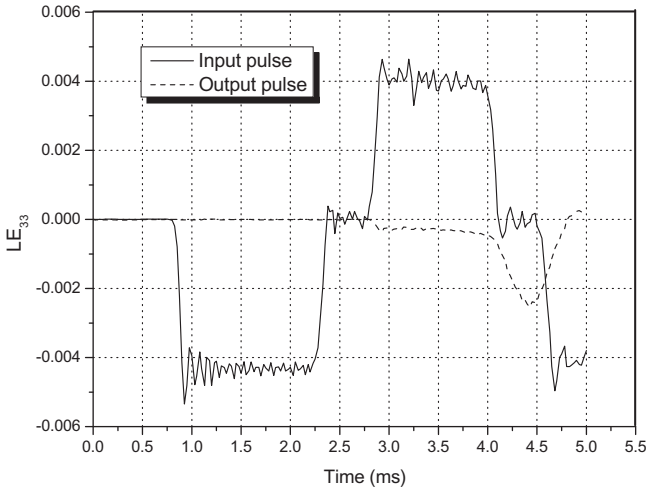

Fig. 6. Input and output pulses tested by nodes at the position of strain gauges.

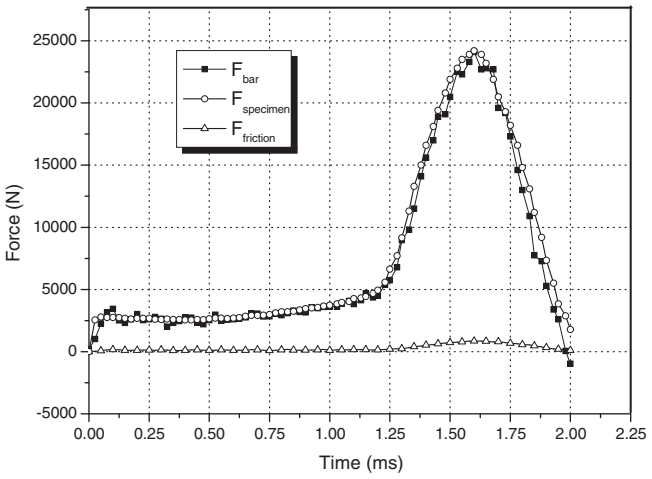

Fig. 8. Comparison between forces.

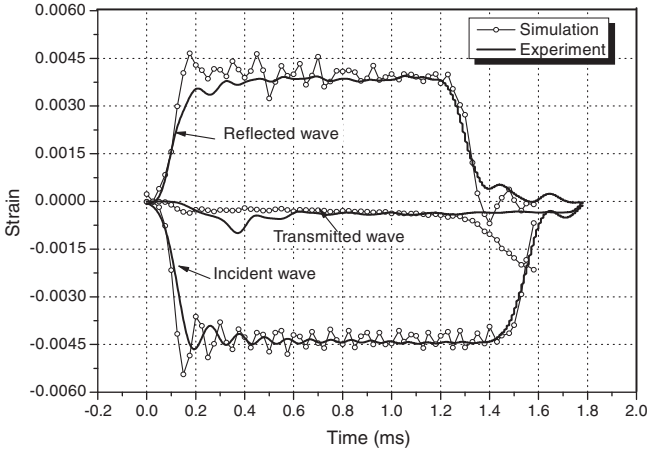

Fig. 7. Comparison of basic waves between simulation and experiment.

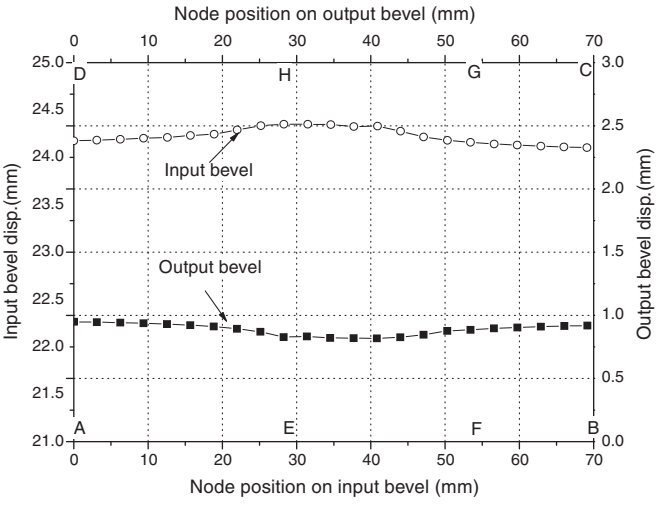

Fig. 9. Displacement on input and output bevels along major axes.

4. Testing results and discussions

4.1. Material and specimen

The hexagonal honeycomb chosen for our experiments is made of aluminum 5052 and possesses a relative density of 3% with single wall thickness $h = 76$ μm, the expansion angle $\alpha = 30°$, and a minimum cell diameter $S = 6.35$ mm. It has three orthotropic directions denoted as T L W (as shown schematically in Fig. 10). The T-direction, also known as the out-of-plane direction corresponds to the axes of the honeycomb cells and is the strongest direction. The other two directions (L and W) are so-called in-plane directions referred as the ribbon direction and the width direction of honeycomb.

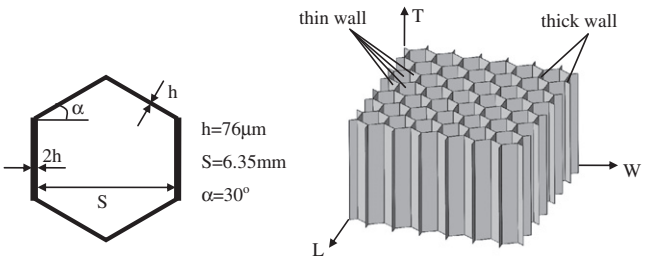

Fig. 10. The geometry of unit cell and the constructed honeycomb specimen.

Cubic specimens are used in dynamic and quasi-static experiments with dimension of 25 × 40 × 40 mm in the directions of T L W respectively which means there are 39 complete cells in the cross section of the honeycomb specimen. There is then more than 6 cells in any direction so that the size effect is normally not important.

4.2. Experimental results

In this study, we performed respectively quasi-static and dynamic experiments at five loading angles in TW loading plane, i.e. 0° for a pure compressive loading, 30°, 40°, 50° and 60° for combined shear-compression loadings.

The quasi-static experiments under combined shear-compression were performed in order to make a dynamic/quasi-static comparison. A universal tension/compression INSTRON3369 machine with the same combined shear-compression device is employed (as shown in Fig. 11). A high-speed camera was used in both quasi-static and dynamic experiments to capture the deformation configuration during the loading process.

4.2.1. Reproducibility

In order to illustrate the reproducibility of the tests, three repeating experiments are conducted for each loading case. Fig. 12 displays the dynamic pressure/crush curves for $\theta = 40°$. The three curves show only a small dispersion indicating that the experimental results are reliable.

4.2.2. Dynamic and quasi-static experimental results

A summary of all dynamic pressure/crush curves in TW plane at five different loading angles is given in Fig. 13.

It is well known that a typical out-of-plane pressure/crush curve of honeycomb under uniaxial compression consists of an initial peak denoting the first plastic collapse of the microstructure, a long stress plateau related to the successive folding process and a densification stage. For all the combined shear-compression tests shown in Fig. 13, the first two stages can be well identified from the curves of our experiments, but the densification stage is absent due to the limitation of loading duration of SHPB.

For these combined shear-compression results, the following observations can be made: First, the slope of the ascending segment to reach the initial peak varies with loading angle θ. Second, the initial peak value decreases with the increase of loading angle θ, which indicates much easier initial collapse of honeycomb at larger loading angle. Third, the average level of the stress plateau becomes lower as the loading angle θ increases.

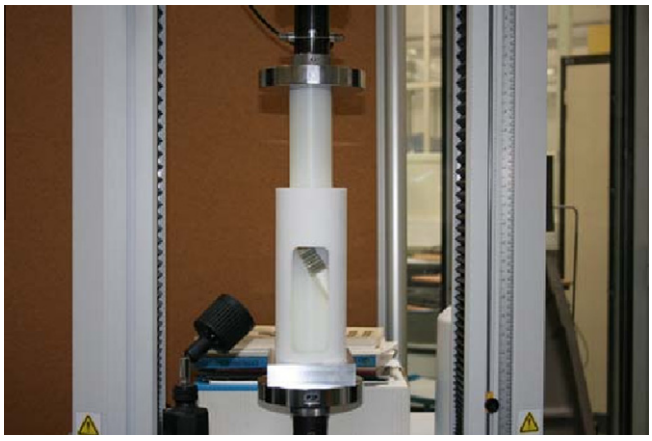

Fig. 11. Photograph of quasi-static loading set-up with INSTRON machine.

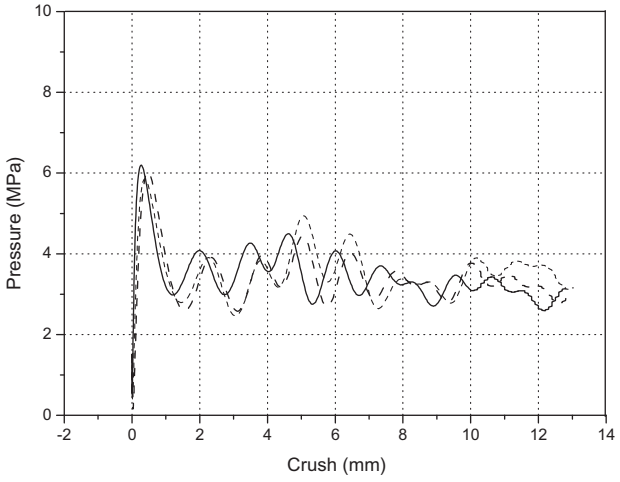

Fig. 12. Reproducibility of impact experiment on honeycomb under combined shear-compression.

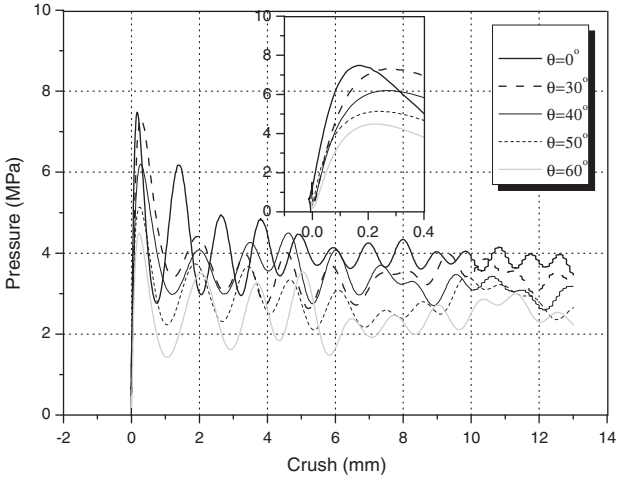

Fig. 13. Dynamic pressure/crush curves in TW plane at different loading angles.

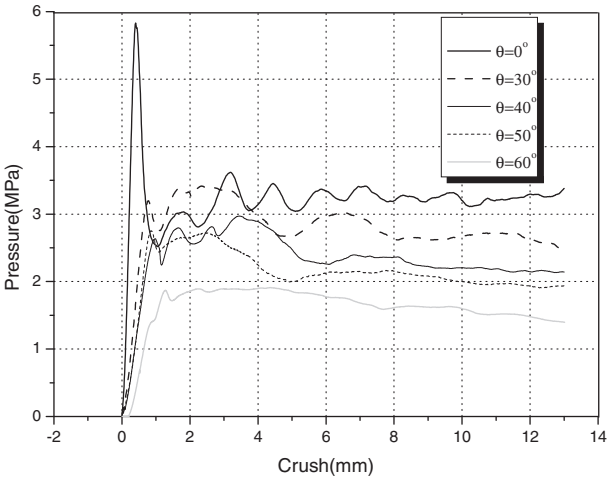

Fig. 14. Quasi-static pressure/crush curves in TW plane at different loading angles.

The experimental results under quasi-static loading are shown in Fig. 14. All the curves are cut off at 13 mm crush in order to facilitate comparison with the dynamic results. It is found that the level of

these quasi-static curves decreases with loading angle, which is similar to the dynamic results. Besides, additional differences with respect to dynamic experiments are found. First, the quasi-static overall pressure/crush curves are smoother than the dynamic ones. Second, the initial peak of quasi-static curves is not as significant as the corresponding dynamic at every combined loading, and the difference of the ascending slope of each curve is much larger than the dynamic results. Further investigation on the deformation details from the captured images reveals a slight slippage between the specimen and the bevels at the beginning of this combined quasi-static shear-compression test. This may cause errors in predicting the properties of honeycomb in the elastic regime for the quasi-static experiments. Finally, as viewed from the plateau level of each curve, the quasi-static ones are all lower than the corresponding dynamic ones, which shows an obvious effect of loading rate.

In order to clarify quantitatively the enhancement from quasi-static to dynamic loading, we compared the quasi-static and dynamic results at two loading stages. Stage I is under elastic deformation from zero crush to the position of initial peak. In this stage, the initial peak values are compared. Stage II covers the rest part of the pressure/crush curves after the initial peak and ends at 13 mm crush. Consequently, we calculated the average strength of stage II by dividing the curve area of this plateau deforming period (absorbed energy) by corresponding crush length, which gives:

$$\bar{p} = \frac{1}{\delta_{\max} - \delta^*} \int_{\delta^*}^{\delta_{\max}} p d\delta, \tag{3}$$

where δ^* denotes the crush value at the point of the initial peak for each of the overall pressure/crush curve. $\delta_{\max}$ is the maximum crush of the corresponding crushing duration, which in this study is taken as 13 mm.

The initial peak values of stage I for both dynamic and quasi-static results are listed in Table 2 and shown in Fig. 15(a). Regardless of the potential errors of the quasi-static results at initial deformation for the combined loading cases, it can be seen that the initial collapse strength of honeycomb under dynamic loading is significantly higher than under quasi-static loadings.

The results of comparison of crushing strength at stage II between dynamic and quasi-static results is also listed in Table 2 and drawn in Fig. 15(b). An enhancement varying from 22% to 48% is found from the dynamic curves to the quasi-static ones.

4.2.3. Discussion

It is worthwhile to reiterate that the tests conducted do provide a combined shear-compression loading because of the friction. The results show that the decrease of the strength with loading angle is rather obvious, however, the measured strength in axis direction (X_3) is not simply equal to the projection of the honeycomb strength under pure compression in this direction. For example, the measured value at 60° is not the half of that at 0° (Table 2).

In fact, the present testing method provides a new way for obtaining the overall behavior of honeycombs under combined shear-compression at various loading angles, which are of much importance for engineering applications. However, further investigation of the multiaxial behavior of cellular materials requires to study the normal and shear behaviors separately. Unfortunately, the normal and shear information on the specimen faces cannot

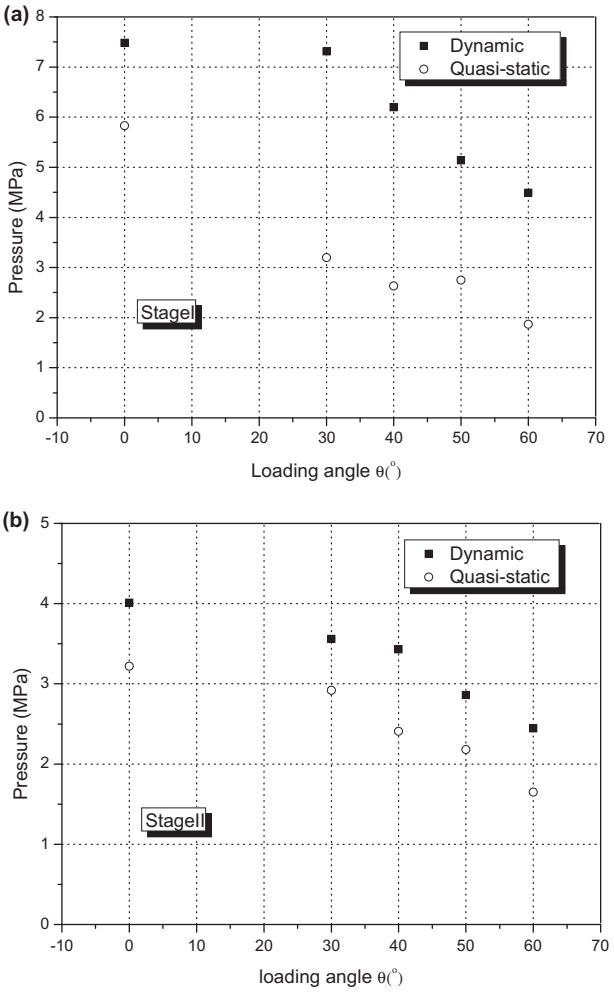

Fig. 15. Comparison between dynamic and quasi-static results in two loading stages.

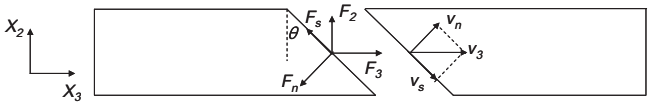

Fig. 16. Scheme of the force balance and the decomposition of velocity.

be obtained directly from the present test set-up. The relationship between the measurable quantities and the normal and shear data on specimen faces are examined hereby.

In Fig. 16, we denote the force and velocity components in global coordinate F_i and $V_i (i = 1,2,3)$. The pressure bars provides F_3 and V_3 in the axial direction. Denoting F_n, V_n and F_s, V_s respectively the forces and velocities applied to specimen faces in normal and shear directions. They are related as follows:

Table 2
Comparison between dynamic and quasi-static loading results.

		0°	30°	40°	50°	60°
Stage I Initial peak (MPa)	Dynamic	7.48	7.31	6.20	5.14	4.49
	Quasi-static	5.83	3.20	2.63	2.75	1.87
Stage II average pressure (MPa)	Dynamic	4.01	3.56	3.43	2.86	2.45
	Quasi-static	3.22	2.92	2.41	2.18	1.65

$$F_1 = 0 \quad V_1 = 0,$$
$$F_2 = F_n \sin\theta - F_s \cos\theta \quad V_2 = 0,$$
$$F_3 = F_n \cos\theta + F_s \sin\theta \quad V_3 = V_n/\cos\theta = V_s/\sin\theta. \tag{3}$$

Under the assumption of identical movements of the beveled ends which was validated in FEM simulations, V_n and V_s can be calculated from a simple expression obtained from the decomposition of V_3. However, the use of the supports in the combined shear-compression device results in the emergence of a transverse reaction force F_2 which is not measurable in the experimental design. Thus, F_n and F_s cannot be calculated from Eq. (3) without knowledge of F_2. Since normal and shear forces applied to the specimen faces are not separable, it is then impossible to determine the multiaxial constitutive relation directly using the present biaxial loading device.

4.2.4. Deformation pattern observations

In our tests, the deformation process of honeycomb under combined shear-compression was captured by high-speed camera. A couple of differences compared with the deforming pattern under uniaxial compression are observed. Fig. 17 presents a series of dynamic deforming patterns of honeycomb under both uniaxial compression and combined shear-compression at $\theta = 30°$. The first images of Fig. 17(a) and (b) correspond to the undeformed configurations. Differences are observed as follows: First, the position of the initial collapse is different (as shown in the images at crush of 0.1 mm). For the uniaxial compression, the collapse initiates at either the top or the bottom face evenly whereas for combined loading occurs simultaneously at the top and bottom faces but in a diagonally corresponding positions. Second, when the specimen

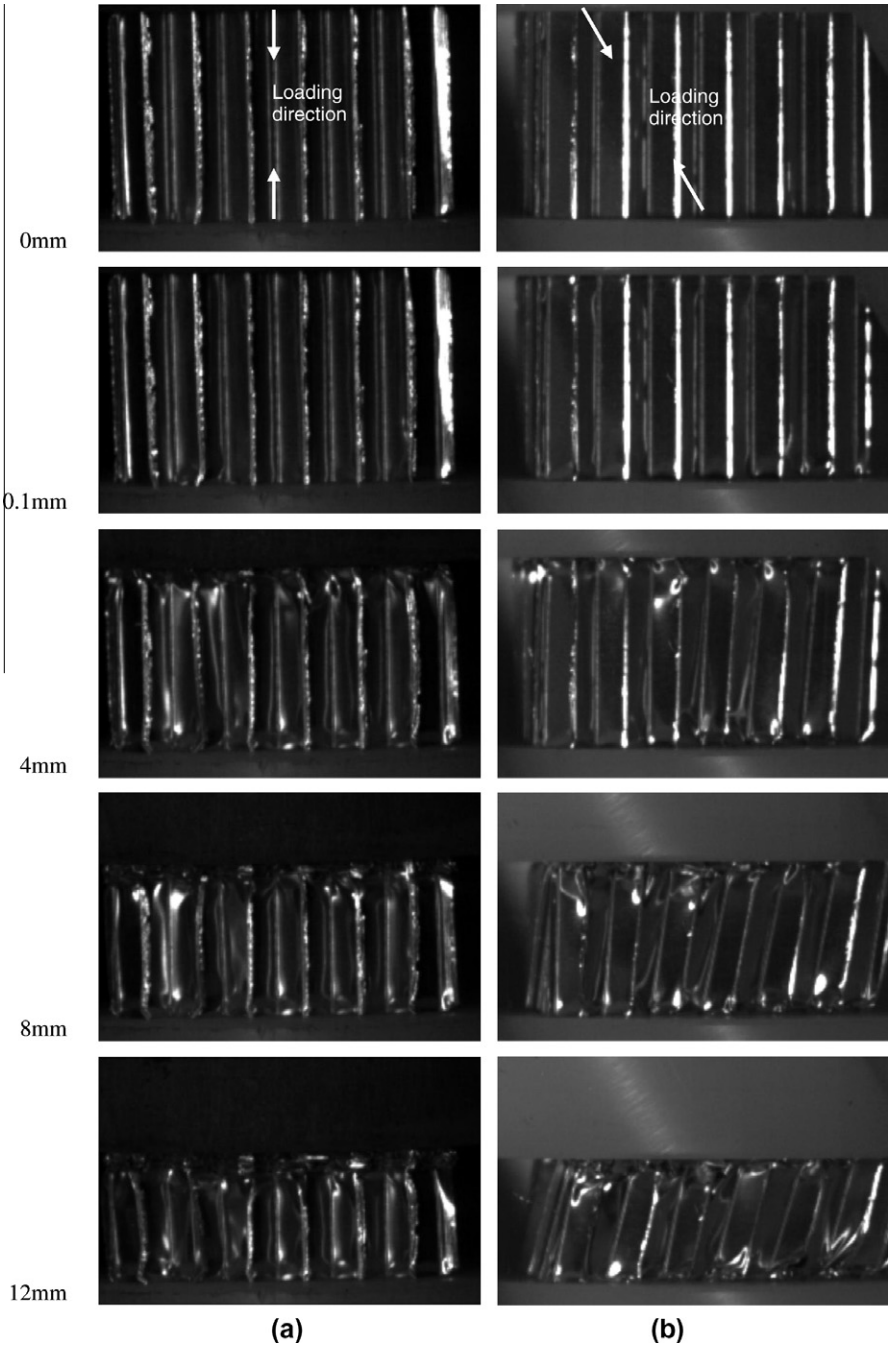

Fig. 17. Dynamic deformation images under uniaxial compression (a) and combined shear-compression at 30° (b) at different crush value.

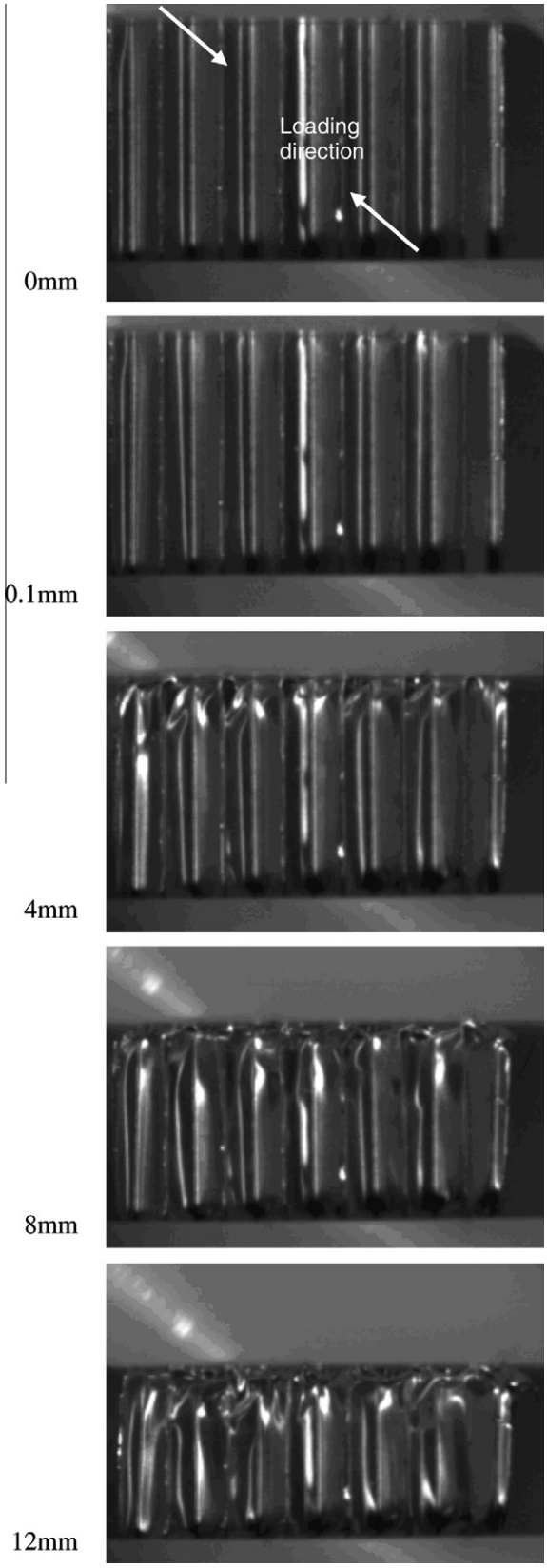

Fig. 18. Another deformation mode of honeycomb under combined dynamic shear-compression found at $\theta = 50°$.

deforms further, the cell axes of the honeycomb specimen under combined loading can incline due to the presence of shear load, while the uniaxial compressive specimen keeps their cell wall axes perpendicular to the loading surfaces.

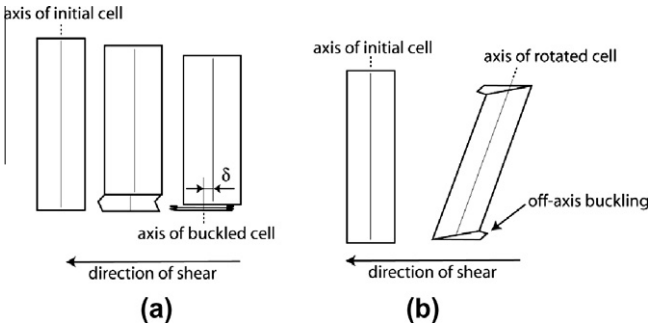

Fig. 19. Deforming modes under shear-compression (a) no rotation, (b) rotation.

This inclined deformation mode was found in most of the combined shear-compression experiments including dynamic and quasi-static loadings. However, for a minority of the specimens under combined shear-compression (even with large loading angle), a deformation mode similar to uniaxial compression was also found. As shown in Fig. 18, one of the specimens at $\theta = 50°$ was crushed from one end of the specimen with the cell wall axes perpendicular to the loading faces. This deforming mode enables a higher loading capacity, which can be seen in the overall pressure/crush curves.

In general, the deforming pattern under combined shear-compression might be summarized as follows: there co-exist two patterns allowing the honeycomb to cope with this prescribed shear-compression loading. One possibility is to maintain the central part with no rotation as for uniaxial compression, but the shear loading induces an overall translation of the buckled cell relative to the non compacted cell (Fig. 19(a)); Another possibility is to allow the rotation of the central part, which is an off-axis local buckling mechanism so that the cells in the central part incline globally during the deformation (Fig. 19(b)). There is a competition of those two different deforming modes during a test.

In order to obtain a general viewpoint of this competition of two deformation modes and especially the influence of the loading rate on it, a quantitative analysis is made by means of indicators taken from the image sequences acquired during experiments at various loading angles. The rotation angle β of the cells during crushing is represented by the angle between the initial orientation of cell axes (perpendicular to the faces of the bevels) and their current orientation. This rotation angle β is a function of mean compressive strain ε which can be defined as the relative variation of specimen length ($\varepsilon = (h_0 - h)/h_0$) as shown in Fig. 20.

Fig. 21 illustrate the rotated angles at $\varepsilon = 40\%$ for all the loading angles under quasi-static as well as dynamic loadings.

It confirms that there is a competition between those two deforming modes. Apart from the tests at 30°, it seems that under quasi-static as well as dynamic loading, there are both possibilities

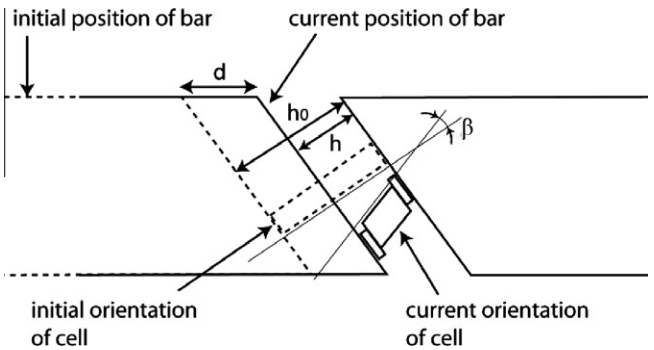

Fig. 20. Scheme for the image analysis.

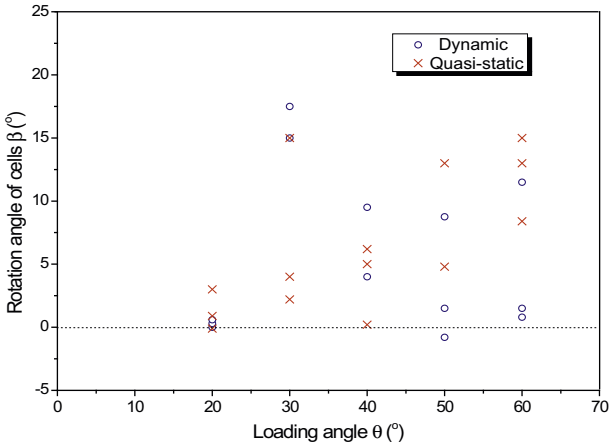

Fig. 21. Rotation angle of cell axes at 40% compression.

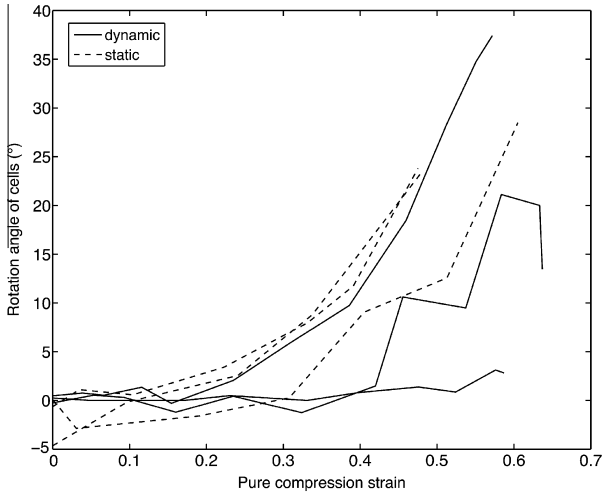

Fig. 22. Rotation angles during tests at a loading angle of 60°.

to remain not rotated or rotate significantly. The larger the loading angle is, the more important the rotation angle becomes. Another rather clear trend is that the probability of rotation is much higher under quasi-static loading than under dynamic loading.

A close look of the case for a loading angle $\theta = 60°$ (most important shear component) is shown in Fig. 22.

It shows that tests at $\theta = 60°$ under dynamic loading mainly remain not rotated whereas tests under quasi-static loading mainly rotate and this is true at any state of crush. Such a difference of deforming modes between quasi-static and dynamic loading might provide an explanation of the enhancement of strength under combined impact shear-compression.

5. Conclusions

In this study, we presented a new combined shear-compression loading method by introducing two short beveled bars into a large-diameter Nylon SHPB set-up and a uniaxial INSTRON machine to investigate the combined shear-compression behavior of honeycomb under dynamic and quasi-static loadings.

The verification of such a design by means of FEM analyses reveals that the force and velocity components in the axial direction of the pressure bar for foam-like specimen under combined shear-compression can be well measured from Hopkinson bar.

The obtained dynamic and quasi-static pressure/crush curves show that both the initial peak value and the average plateau strength decrease significantly with increasing loading angle. An enhancement of these values is found for dynamic curves compared to quasi-static ones at every loading angle. From high-speed photographs, the difference of the deformation mode under uniaixal compression from this combined shear-compression is identified. It allows also to reveal the two co-existing deformation modes under combined shear-compression and the influence of loading rate on the competition of these two deforming modes.

The combined shear-compression loading device presented in this paper provides an overall behavior of cellular materials under these multiaxial loading conditions but it cannot give directly the separated normal and shear components of the behavior. A numeric method will be presented in Part II of this work in order to overcome this difficulty. acknowAcknowledgementThe authors thank 111 project of China (contract No.1307050) for funding the cooperation between NPU and LMT. B. Hou and Y. L. Li would also like to thank the supports of the National Science Foundation of China (contract No.10932008).

References

Chen, C., Fleck, N.A., 2002. Size effects in the constrained deformation of metallic foams. J. Mech. Phys. Solids 50, 955–977.
Chen, W.N., Ravichandran, G., 1997. Dynamic compressive failure of a glass ceramic under lateral confinement. J. Mech. Phys. Solids 45, 1303–1328.
Chung, J., Waas, A.M., 2002. Compressive response of circular cell polycarbonate honeycombs under inplane biaxial static and dynamic loading. Part I: experiments. Int. J. Impact Eng. 27, 729–754.
Deshpand, V.S., Fleck, N.A., 2001. Multi-axial yield behaviour of polymer foams. Acta Mater. 49, 1859–1866.
Gary, G., Bailly, P., 1998. Behaviour of quasi-brittle material at high strain rate, experiment and modeling. Eur. J. Mech, A/Solids 17 (3), 403–420.
Goldsmith, W., Louie, D.L., 1995. Axial perforation of aluminum honeycombs by projectiles. Int. J. Solids Struct. 32, 1017–1046.
Hong, S.T., Pan, J., Tyan, T., Prasad, P., 2006. Quasi-static crush behavior of aluminum honeycombs specimens under compression dominant combined loads. Int. J. Plast. 22, 73–109.
Hong, S.T., Pan, J., Tyan, T., Prasad, P., 2008. Dynamic crush behaviors of aluminum honeycomb specimens under compression dominant inclined loads. Int. J. Plast. 24, 89–117.
Hopkinson, B., 1914. A method of measuring the pressure in the deformation of high explosives by the impact of bullets. Phil. Trans. Roy. Soc. A213, 437–452.
Karagiozova, D., Yu, T.X., 2008. Strain localization in circular honeycombs under in-plane biaxial quasi-static and low-velocity impact loading. Int. J Impact Eng. 35, 753–770.
Kintscher, M., Kärger, L., Wetzel, A., Hartung, D., 2007. Stiffness and failure behaviour of folded sandwich cores under combined transverse shear and compression. Compos. Part A 38, 1288–1295.
Kolsky, H., 1949. An investigation of the mechanical properties of materials at very high rates of loading. Proc. Phys. Soc. B62, 676–700.
Mohr, D., Doyoyo, M., 2002. Analysis of the Arcan apparatus in the clamped configuration. J. Compos. Mater. 36, 2583–2594.
Mohr, D., Doyoyo, M., 2003. A new method for the biaxial testing of cellular Solids. Exp. Mech. 43 (2), 174–183.
Mohr, D., Doyoyo, M., 2004. Experimental investigation on the plasticity of hexagonal aluminum honeycomb under multiaxial loading. J. Appl. Mech. 71, 375–385.
Nie, X., Chen, W.W., Sun, X., Templeton, D.W., 2007. Dynamic failure of borosilicate glass under compression/shear loading-experiments. J. Amer. Ceram. Soc. 90 (8), 2362–2556.
Papka, S.D., Kyriakides, S., 1999. Biaxial crushing of honeycombs – Part I: experiments. Int. J. Solids Struct. 36, 4367–4396.
Rae, P.J., Dattelbaum, D.M., 2004. The properties of poly (tetrafluoroethylene) (PTFE) in compression. Polymer 45, 7615–7625.
Rittel, D., Lee, S., Ravichandran, G., 2002. A shear-compression specimen for large strain testing. Exp. Mech. 42 (1), 58–64.
Wierzbicki, T., 1983. Crushing analysis of metal honeycombs. Int. J. Impact Eng. 1, 157–174.
Wu, E., Jiang, W.S., 1997. Axial crush of metallic honeycombs. Int. J. Impact Eng. 19, 439–456.
Zhang, J., Ashby, M.F., 1992. The out-of-plane properties of honeycombs. Int. J. Mech. Sci. 34, 475–489.
Zhao, H., 1997. A constitutive model for metals over a large range of strain rates, Identification for mild-steel and aluminium sheets. Mater. Sci. Eng. A320, 95–99.

Zhao, H., 1998. A study of specimen thickness effects in the impact tests on polymers by numeric simulations. Polymer 39, 1103–1106.
Zhao, H., Gary, G., 1998. Crushing behaviour of aluminium honeycombs under impact loading. Int. J. Impact Eng. 21, 827–836.
Zhao, H., Gary, G., Klepaczko, J.R., 1997. On the use of viscoelastic split Hopkinson pressure bar. Int. J. Impact Eng. 19, 319–330.
Zhao, H., Elnasri, I., Abdennadher, S., 2005. An experimental study on the behavior under impact loading of metallic cellular materials. Int. J. Mech. Sci. 47, 757–774.